

## ***In-situ* XAS study of catalytic N<sub>2</sub>O decomposition over CuO/CeO<sub>2</sub> catalysts**

Maxim Zabitskiy<sup>[a]</sup>, Iztok Arčon<sup>[b,c]</sup>, Petar Djinić<sup>[d]</sup>, Elena Tchernychova<sup>[e]</sup>, Albin Pintar<sup>[d]</sup>

[a] Dr. M. Zabitskiy  
Laboratory for Catalysis and Sustainable Chemistry,  
Paul Scherrer Institute,  
CH-5232 Villigen, Switzerland  
E-mail: [maxim.zabitskiy@psi.ch](mailto:maxim.zabitskiy@psi.ch)

[b] Prof. Dr. I. Arčon  
Laboratory of Quantum Optics,  
University of Nova Gorica,  
Vipavska 13, SI-5000 Nova Gorica, Slovenia  
E-mail: [iztok.arcon@ung.si](mailto:iztok.arcon@ung.si)

[c] Prof. Dr. I. Arčon  
Department of Low and Medium Energy Physics,  
Jožef Stefan Institute,  
Jamova 39, SI-1001 Ljubljana, Slovenia

[d] Dr. P. Djinić, Dr. A. Pintar  
Department of Inorganic Chemistry and Technology,  
National Institute of Chemistry,  
Hajdrihova 19, SI-1001 Ljubljana, Slovenia

[e] Dr. E. Tchernychova  
Department for Materials Chemistry,  
National Institute of Chemistry,  
Hajdrihova 19, SI-1001 Ljubljana, Slovenia

**Abstract** – We performed *in-situ* XAS study of N<sub>2</sub>O decomposition over CuO/CeO<sub>2</sub> catalysts.

The Cu K-edge and Ce L<sub>3</sub>-edge XANES and EXAFS analyses revealed the dynamic and crucial role of Cu<sup>2+</sup>/Cu<sup>+</sup> and Ce<sup>4+</sup>/Ce<sup>3+</sup> ionic pairs during the catalytic reaction. We observed the initial formation of reduced Cu<sup>+</sup> and Ce<sup>3+</sup> species during activation in helium atmosphere at 400 °C, while concentration of these species decreased significantly during steady-state nitrous oxide degradation reaction (2500 ppm N<sub>2</sub>O in He at 400 °C). *In-situ* EXAFS analysis further revealed a crucial role of copper-ceria interface in this catalytic reaction. We observed dynamic changes in average number of Cu-Ce scatters under reaction conditions, indicating

an enlarging the interface between both copper and ceria phases, where electron and oxygen transfer occurs.

**Keywords:** N<sub>2</sub>O decomposition; CuO/CeO<sub>2</sub> nanorod catalyst; *in-situ* XAS; Cu<sup>+</sup>/Cu<sup>2+</sup> and Ce<sup>3+</sup>/Ce<sup>4+</sup> redox pairs; copper-ceria interface

## 1. Introduction

Nitrous oxide (N<sub>2</sub>O) is a principal anthropogenic pollutant and one of the strongest greenhouse gases, which has a high global warming potential (310 times higher compared to CO<sub>2</sub>) and a long atmospheric lifetime (half-life decomposition period of N<sub>2</sub>O is approximately 120 years).<sup>[1,2]</sup> Estimated amount of N<sub>2</sub>O emissions into the Earth atmosphere as a result of human activities is 5.3 Mt N<sub>2</sub>O-N yr<sup>-1</sup> (megatons of N<sub>2</sub>O in equivalent nitrogen units per year), from which industrial sector (nitric acid, adipic acid, and caprolactam production) and fossil fuel combustion account for approximately 15 % of total gross anthropogenic N<sub>2</sub>O emissions.<sup>[3]</sup> Therefore, the development of an appropriate heterogeneous catalyst that can efficiently decompose N<sub>2</sub>O from industrial emissions to environmentally benign O<sub>2</sub> and N<sub>2</sub> at low temperatures is highly required.

Among the vast variety of heterogeneous catalyst formulations: noble metals based catalysts<sup>[4-8]</sup>, metal oxides and mixed metal oxides,<sup>[9-12]</sup> zeolite based materials,<sup>[13,14]</sup> spinels<sup>[15-17]</sup> and perovskites,<sup>[18,19]</sup> CuO/CeO<sub>2</sub> catalyst can be considered as a suitable candidate for the abovementioned process commercialization due to its high activity, long-term stability and favorable price (copper is significantly cheaper compared to noble metals).<sup>[20-24]</sup> In our recent works,<sup>[20-22]</sup> we have shown that exceptional catalytic activity of the CuO/CeO<sub>2</sub> system originates from the synergetic electronic interactions between copper and ceria phases, which

promote metal-oxygen bond weakening, facilitate oxygen desorption and promote the active site regeneration. By using a suitable synthesis technique,<sup>[21]</sup> we were able to synthesize ceria supports having various morphological forms (nanocubes, nanorods, and polyhedral nanoparticles), which expose different surface planes. We have shown by XPS and TEM-EELS techniques,<sup>[25]</sup> that exceptional catalytic activity of copper oxide supported on ceria having nanorod shape and predominantly exposing {100} and {110} surface planes correlates well with the enrichment of the nanorod's surface with reduced  $\text{Ce}^{3+}$ . The latter can be attributed to the improved reducibility and oxygen mobility of ceria nanorod support.<sup>[26]</sup> At the same time, we have observed the formation of  $\text{Cu}^+$  species by using CO as a probe molecule by DRIFTS.<sup>[21,25]</sup> XPS measurements also identified that copper is predominantly present as  $\text{Cu}^+$ .<sup>[21]</sup> The *in-situ* UV-Vis DR study<sup>[25]</sup> suggested that both  $\text{Ce}^{3+}/\text{Ce}^{4+}$  and  $\text{Cu}^+/\text{Cu}^{2+}$  ionic pairs participate in the catalytic cycle of  $\text{N}_2\text{O}$  decomposition over  $\text{CuO}/\text{CeO}_2$ . Based on the abovementioned results, we postulated that the synergetic effect between both oxide phases plays a crucial role in catalytic activity and the  $\text{Ce}^{3+}/\text{Ce}^{4+}$  and  $\text{Cu}^+/\text{Cu}^{2+}$  synergy should be investigated in detail in order to allow further catalyst modification and activity improvement.

XPS and TEM-EELS examinations used in our previous studies were done in *ex-situ* mode under ultra high-vacuum (UHV) and ambient temperature, which is far away from the realistic  $\text{N}_2\text{O}$  decomposition conditions (400 °C and 1 bar). The UHV and electron beam-damage by themselves may lead to catalyst reduction and enrichment of the catalyst surface with reduced  $\text{Cu}^+$  and  $\text{Ce}^{3+}$  species. Furthermore, the presence of  $\text{Cu}^+$  and  $\text{Ce}^{3+}$  under *ex-situ* conditions does not necessarily guarantee the participation of these  $\text{Ce}^{3+}/\text{Ce}^{4+}$  and  $\text{Cu}^+/\text{Cu}^{2+}$  ionic pairs in the catalytic cycle under realistic catalytic experiment. This motivated us to perform *in-situ* XAS catalyst characterization and investigate the synergetic effect between  $\text{CuO}$  and  $\text{CeO}_2$  phases under relevant  $\text{N}_2\text{O}$  decomposition conditions (400 °C and 1 bar).

In the present work, we investigated a series of CuO/CeO<sub>2</sub> catalysts containing 2-8 wt. % of Cu supported on CeO<sub>2</sub> nanorods, nanocubes and polyhedral nanoparticles during *in-situ* catalytic N<sub>2</sub>O decomposition by using XAS (Cu K-edge and Ce L<sub>3</sub>-edge). We have found that both Cu<sup>+</sup>/Cu<sup>2+</sup> and Ce<sup>3+</sup>/Ce<sup>4+</sup> ionic pairs participate in the catalytic cycle of N<sub>2</sub>O decomposition. Furthermore, results of EXAFS analysis revealed the crucial role of the copper-ceria interface, which is responsible for the enhanced activity of this catalyst.

## 2. Experimental

### 2.1. Catalyst synthesis

Synthesis of nanoshaped CeO<sub>2</sub> supports was adopted from our previous work.<sup>[21]</sup> For synthesis of ceria nanocubes – CeO<sub>2</sub>-C and nanorods – CeO<sub>2</sub>-R, 53.8 g of NaOH (99% purity, Merck) was dissolved in 140 mL of deionized water. For polyhedral ceria nanoparticles – CeO<sub>2</sub>-P, 8.96 g of NaOH was used. This alkaline solution was added under stirring to an aqueous solution containing 4.9 g of Ce(NO<sub>3</sub>)<sub>3</sub>·6H<sub>2</sub>O (99% purity, Sigma-Aldrich) dissolved in 84 mL of deionized water. After 30 min of stirring at ambient temperature, the suspension was transferred into a Teflon-lined stainless steel autoclave. The following conditions were applied during hydrothermal treatment step: i) 24 h at 180 °C for CeO<sub>2</sub>-C, or ii) 24 h at 100 °C for CeO<sub>2</sub>-R and CeO<sub>2</sub>-P samples. After cooling, the suspensions were centrifuged at 5000 rpm and thoroughly washed with excess of deionized water until reaching pH=7. The obtained solids were dried for 24 h using a freeze-dryer (Christ, model Alpha 1-2 LDplus). Finally, ceria powder precursors were calcined at 400 °C for 3 h in air (heating ramp 2 °C/min).

Between 2 and 8 wt. % of Cu was deposited on ceria supports by precipitation method

accordingly to the following protocol: 500 mg of nanoshaped ceria support was dispersed in 10 mL of deionized water followed by addition of an appropriate amount of  $\text{Cu}(\text{NO}_3)_2 \cdot 3\text{H}_2\text{O}$  (99.5% purity, Sigma-Aldrich) corresponding to the desired nominal copper loading. In the next step, 250 mg of  $\text{Na}_2\text{CO}_3$  (99.999% purity, Merck) was dissolved in 5 mL of deionized water and added under vigorous stirring. The formed suspension was stirred for additional 2 h at ambient temperature. Then, the solid was filtered, washed with an excess of deionized water until reaching  $\text{pH}=7$  and dried for 24 h using a freeze drier. The obtained catalyst precursor was calcined at  $400^\circ\text{C}$  for 3 h in air. The synthesized  $\text{CuO}/\text{CeO}_2$  catalysts were marked as  $\text{XCu}_-\text{CeO}_2\text{-M}$ , where X identifies the nominal copper content and M represents the ceria shape: R for rods, C for cubes and P for polyhedra).

## 2.2. Catalyst characterization

Measurements of BET specific surface area, total pore volume and pore size distribution were performed at  $-196^\circ\text{C}$  using a TriStar II 3020 instrument from Micromeritics.

Particle size and morphology were studied by means of high-resolution transmission electron microscopy (HRTEM) and scanning TEM high-angle annular dark field imaging (STEM-HAADF). Copper distribution was assessed by energy-dispersive X-ray spectroscopy in STEM mode (STEM-EDX). For these analyses, a probe aberration-corrected JEM-ARM200CF equipped with the JEOL Centurio 100  $\text{mm}^2$  EDXS detector and JEOL STEM detectors (JEOL, Tokyo, Japan) was employed.

X-ray diffraction (XRD) measurements were performed at room temperature on a Bruker D8 Advance AXS diffractometer using  $\text{Cu } K_{\alpha 1}$  radiation with  $\lambda=0.15406$  nm. Materials were scanned in the  $2\theta$  range between  $20$  and  $65^\circ$  with  $0.021^\circ$  increment and 1 s acquisition time at each point. Scherrer equation was applied to the most intensive 111 diffraction peak of ceria

to estimate its average scattering domain size.

The N<sub>2</sub>O chemisorption protocol used for the calculation of copper dispersion and Cu average size was similar to that described in our previous study.<sup>[21]</sup> Experiments were performed using a Micromeritics AutoChem II 2920 apparatus. In a typical experiment the investigated sample (approximately 100 mg) was firstly pre-reduced in 5 vol. % H<sub>2</sub>/Ar mixture at 300 °C (heating ramp 5 °C/min). To selectively probe only metallic copper surface sites and avoid titration of oxygen defect sites of CeO<sub>2</sub> support and over-oxidation of bulk Cu phase, N<sub>2</sub>O pulsing (0.5 ml 10 vol. % N<sub>2</sub>O/He) was performed at 35 °C.

Decomposition of N<sub>2</sub>O and formation of N<sub>2</sub> were monitored using a TCD detector (a liquid nitrogen cold trap was mounted before a TCD detector in order to condense unreacted N<sub>2</sub>O, so only N<sub>2</sub> formed during N<sub>2</sub>O pulse titration was detected by the TCD detector). The amount of consumed N<sub>2</sub>O during selective oxidation of Cu surface sites was quantified by using Peak editor software from Micromeritics. Assuming a stoichiometry of N<sub>2</sub>O/Cu<sub>surface</sub>= 1:2, Cu dispersion ( $D_{Cu} = Cu_{(surface)}/Cu_{total}$ ) was determined accordingly to Equation 1:

$$D_{Cu} = \frac{2 \cdot n(N_2O)}{n(Cu)} \quad (1)$$

where  $n(N_2O)$  is the amount of consumed N<sub>2</sub>O during pulse experiment and  $n(Cu)$  is the total amount of Cu in examined CuO/CeO<sub>2</sub> solid. The average crystallite size of supported Cu was determined accordingly to Equation 2 assuming spherical morphology of Cu nanoparticles<sup>[27,28]</sup>:

$$d_{Cu} = \frac{6 \cdot v_m}{D_{Cu} \cdot a_m} = \frac{1.1}{D_{Cu}} \quad (2)$$

where  $v_m$  is the volume occupied by a Cu atom,  $D_{Cu}$  is Cu dispersion and  $a_m$  is the surface area occupied by an exposed surface Cu atom.

### 2.3. Catalytic $N_2O$ decomposition

50 mg of CuO/CeO<sub>2</sub> catalyst diluted with 200 mg of SiC was positioned inside the quartz tube (inner diameter of 9 mm) and fixed between two quartz wool beads. Prior to the catalytic test, the sample was heated (2 °C/min) and activated *in-situ* (Ar, purity 6.0, 50 mL/min) at 400 °C for 2 h. N<sub>2</sub>O decomposition test was performed in the temperature range between 300 and 550 °C and 1 bar. After catalyst activation, 2500 ppm of N<sub>2</sub>O (balanced by Ar) was fed to the reactor, keeping the gas flow rate equal to 100 mL/min (WHSV=120 L/(g<sub>cat</sub>·h)). Remaining N<sub>2</sub>O, as well as products of its catalytic decomposition (O<sub>2</sub> and N<sub>2</sub>) were measured at the reactor outlet by using a micro GC (Agilent Technologies, model 490) equipped with MS5A (10 m) and Porabond Q (10 m) columns. According to the quantitative GC analysis, the evolution of N<sub>2</sub> and O<sub>2</sub> is quantitatively coupled with the N<sub>2</sub>O decomposition stoichiometry in the temperature range 300 – 550 °C.

### 2.4. *In-situ* XAS experiment

*In-situ* Ce L<sub>3</sub>-edge (5724 eV) and Cu K-edge (8979 eV) XANES and EXAFS spectra were measured in transmission detection mode on a set of CuO/CeO<sub>2</sub> catalysts with different ceria morphologies: nanocubes (CeO<sub>2</sub>-C) and nanorods (CeO<sub>2</sub>-R) with Cu loadings ranging between 2 and 8 wt.%. The experiments were performed at the XAFS beamline of the ELETTRA synchrotron radiation facility in Trieste, Italy, and at the P65 beamline of PETRA III, DESY, Hamburg, Germany. A Si (111) double crystal monochromator was used with

energy resolution of about 1 eV at 9 keV (0.6 eV at 6 keV). At the P65 beamline, higher-order harmonics were effectively eliminated by the flat mirror installed in front of the monochromator. The size of the beam on the sample was about 1 mm in diameter. At XAFS beamline the higher harmonics were eliminated by detuning of the second monochromator crystal to 60% of the maximum in the rocking curve, and the size of the beam on the sample was set to about 1 mm  $\times$  3 mm. The intensity of the monochromatic X-ray beam was measured by three consecutive ionization detectors filled with optimal gas mixtures for a given energy range. At P65 beamline, 5cm long ionization chambers were used. For Cu K-edge, the cells were filled with: 1000 mbar N<sub>2</sub> (first), 1000 mbar Ar (second), and 1000 mbar Kr (third). At XAFS beamline 30 cm long ionization chambers were used. For Cu K-edge the cells were filled with gas mixtures: 1250 mbar N<sub>2</sub> and 750 mbar He (first); 250 mbar Ar, 1000 mbar N<sub>2</sub> and 750 mbar He (second); 1000 mbar N<sub>2</sub>, 300 mbar He and 700 mbar Ar (third). For Ce L<sub>3</sub>-edge the cells were filled with gas mixtures: 350 mbar N<sub>2</sub> and 1650 mbar He (first); 1900 mbar N<sub>2</sub> and 100 mbar He (second); 230 mbar Ar, 1000 mbar N<sub>2</sub> and 670 mbar He (third).

The catalyst samples were prepared in the form of homogeneous pellets, pressed from micronized powder mixed with micronized BN, with the total absorption thickness of about 2 above the Cu K-edge or Ce L<sub>3</sub>-edge, and inserted in a tubular oven reactor with 20 micron aluminum windows, filled with protective He atmosphere at 1 bar. Sample pellets, closed in a tubular oven reactor, were placed in the monochromatic beam between the first two ionization detectors. XAS spectra were measured *in-situ*, at room temperature, during heating in He, at 400 °C in He, and during the catalytic reaction in 2500 ppm of N<sub>2</sub>O in He at 1 bar and 400 °C. The absorption spectra were measured in the energy region from -150 eV to +1000 eV relative to the Cu K-edge, while for Ce L<sub>3</sub>-edge EXAFS scans were stopped at Ce L<sub>2</sub>-edge (6165 eV). At XAFS beamline equidistant energy steps of 0.3 eV were used in the XANES

region, while for the EXAFS region equidistant  $k$  steps of  $0.03 \text{ \AA}^{-1}$  were adopted, with an integration time of 2 s/step. At P65 beamline fast (3 min) continuous scans were performed and re-binned to the same energy steps as at XAFS beamline.

In each stationary state, two to five repetitions of the scans were measured and superimposed to improve the signal-to-noise ratio. The XAS scans were measured on different spots of the sample pellet to reduce eventual effects of radiation damage. The exact energy calibration was established with simultaneous absorption measurement on a 7 micron thick Cu metal foil for Cu K-edge, or CeO<sub>2</sub> reference sample (calibrated with vanadium metal foil) for Ce L<sub>3</sub>-edge, placed between the second and the third ionization chamber. Absolute energy reproducibility of the measured spectra was  $\pm 0.03 \text{ eV}$ .

The quantitative analysis of XANES and EXAFS spectra was performed with the Demeter (IFEFFIT) program package,<sup>[29]</sup> in combination with FEFF6 program code for *ab initio* calculation of photoelectron scattering paths.<sup>[30]</sup> Details about XAS experiment are given in supplementary materials.

### 3. Results and discussion

#### 3.1. Material characterization and catalytic N<sub>2</sub>O decomposition

As confirmed by TEM investigation (Figures 1 and S1), the CeO<sub>2</sub>-C sample is composed of nanoparticles having cubic morphology with an average particle size being 20 nm. The ceria nanorods (CeO<sub>2</sub>-R) had on average a diameter of 8 nm and length between 80 and 140 nm. The ceria nanoparticles (CeO<sub>2</sub>-P) measured on average 6.5 nm. Each ceria support shape influences the Cu distribution: being most dispersed over CeO<sub>2</sub>-P sample, clustered and amorphous over CeO<sub>2</sub>-R, and mostly crystalline with rather large crystallite sizes in case of

CeO<sub>2</sub>-C sample (Figure 1).

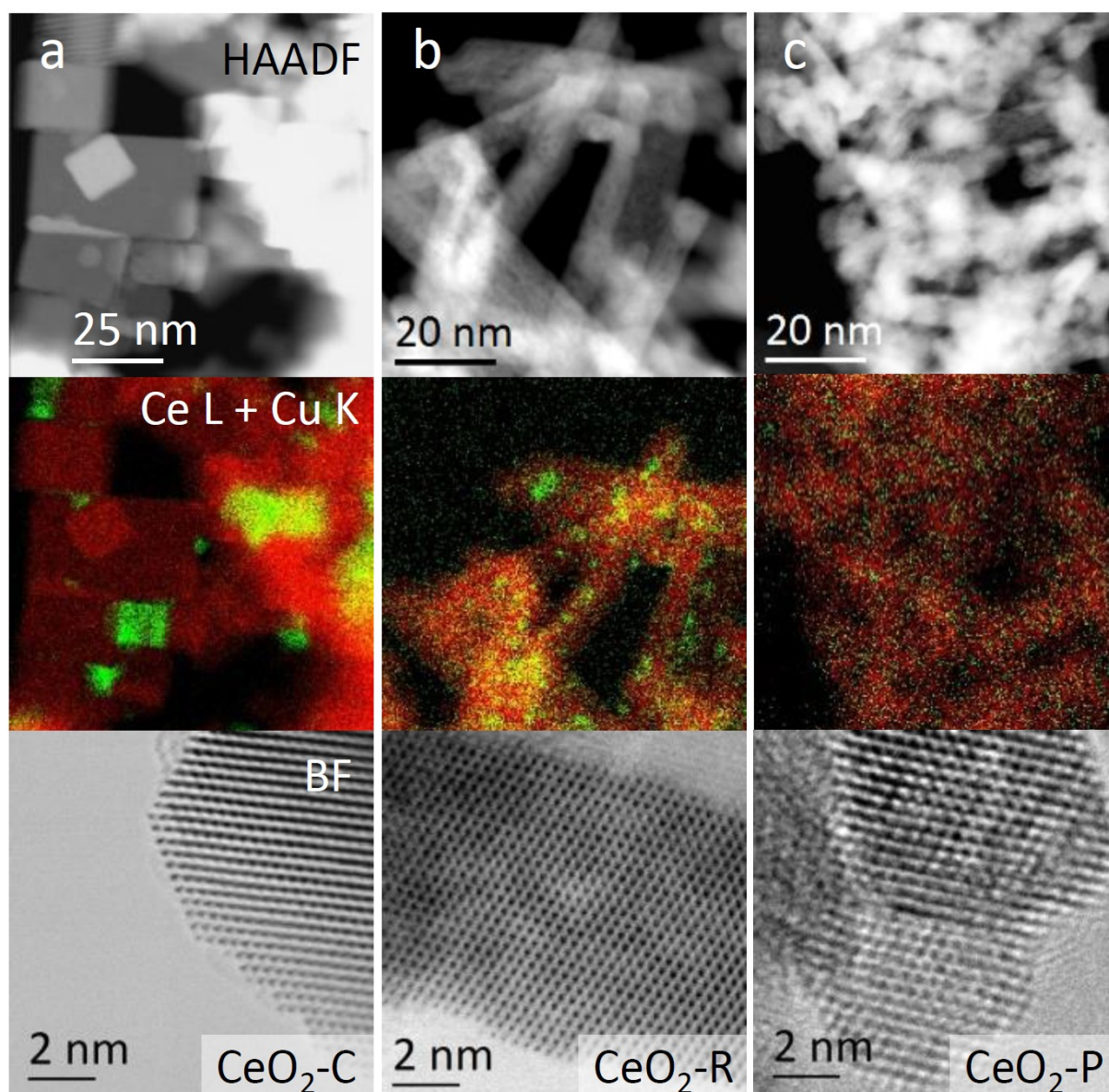


**Figure 1.** STEM-HAADF, STEM-EDX Ce L (red color) and Cu K (green color) line maps, and atomic resolution BF-STEM images of a) CeO<sub>2</sub>-C, b) CeO<sub>2</sub>-R and c) CeO<sub>2</sub>-P samples containing 4 wt.% of copper.

**Table 1.** Structural analysis and catalytic performance of CuO/CeO<sub>2</sub> catalysts containing 4 wt. % copper.

Sample	S <sub>BET</sub> , m <sup>2</sup> /g	<sup>a</sup> d <sub>CeO<sub>2</sub></sub> , nm	<sup>b</sup> d <sub>Cu</sub> , nm	<sup>c</sup> D <sub>Cu</sub> , %	<sup>d</sup> T <sub>50</sub> , °C	<sup>e</sup> TOF, min <sup>-1</sup>
4-Cu_CeO <sub>2</sub> -C	33	27	5.1	22	470	0.130
4-Cu_CeO <sub>2</sub> -R	88	11	2.4	46	430	0.138
4-Cu_CeO <sub>2</sub> -P	110	8	2.1	52	440	0.111

<sup>a</sup>Crystallite size of ceria calculated using Scherrer equation. <sup>b</sup>Average particle size of copper and <sup>c</sup>dispersion of copper measured by means of dissociative N<sub>2</sub>O adsorption. <sup>d</sup>Temperature corresponding to 50 % of N<sub>2</sub>O conversion. <sup>e</sup>Turnover frequency was calculated by dividing moles of decomposed N<sub>2</sub>O at T=375 °C by moles of surface Cu atoms per unit time.

The results of the structural analysis of CuO/CeO<sub>2</sub> catalysts and their catalytic activity are summarized in Table 1. Likely, due to the relatively low specific BET surface area of CeO<sub>2</sub>-C support, the dispersion of copper for this sample is only 22 %, corresponding to an average particle size of copper being 5.1 nm. On the other hand, CeO<sub>2</sub>-R and CeO<sub>2</sub>-P based samples possessing 88 and 110 m<sup>2</sup>/g of surface area, respectively, prevent copper oxide nanoparticles agglomeration during deposition and calcination steps, which results in very similar particle size of copper, i.e. 2.4 and 2.1 nm, respectively. The CeO<sub>2</sub> particle size estimated by XRD and TEM techniques is very similar, so we can conclude that the size distribution of ceria nanoparticles is narrow and the visualized ceria particles are single crystals. The average crystallite size obtained by XRD is an average value obtained from a relatively large amount of sample probed. The size estimation by TEM analysis is statistically less robust, as it is obtained from a very small amount of sample (very localized analysis).

Results of catalytic N<sub>2</sub>O decomposition over catalysts containing 4 wt. % copper are presented in Figure 2. The 4-Cu\_CeO<sub>2</sub>-C sample containing larger copper oxide particles

shows significantly lower  $\text{N}_2\text{O}$  conversion. As it was stressed in our previous research,<sup>[22]</sup> particle size of copper oxide significantly influences overall activity and small CuO clusters enable a higher rate of  $\text{N}_2\text{O}$  decomposition compared to the bulk CuO phase. The 4-Cu\_CeO<sub>2</sub>-R and 4-Cu\_CeO<sub>2</sub>-P samples showed very similar  $\text{N}_2\text{O}$  conversion profiles. In spite of smaller average particle size of copper phase on 4-Cu\_CeO<sub>2</sub>-P, the 4-Cu\_CeO<sub>2</sub>-R sample slightly outperforms the CeO<sub>2</sub>-P based catalyst and shows higher  $\text{N}_2\text{O}$  conversion in the range of 375-550 °C. To verify the size dependent catalytic activity, we have calculated turnover frequencies for these three catalysts at 400 °C (Table 1). Interestingly, there is no correlation between TOF values and copper particle size, revealing the reaction rate (or the rate-determining step) is not determined by the copper nanoparticle alone, but more likely with the copper ceria interface. The terminating facets of ceria are characterized by different energies for oxygen vacancy formation (2.60, 1.99 and 2.27 eV on 111, 110 and 100, respectively<sup>[31]</sup>), and consequently different reactivity and mobility of surface oxygen. The ceria nanocube and nanorod based materials with exposed {100} and {110} surface planes (less thermodynamically stable compared to {111} planes of polyhedral ceria) possess about 25 % higher activity per copper site compared to the 4-Cu\_CeO<sub>2</sub>-P sample.

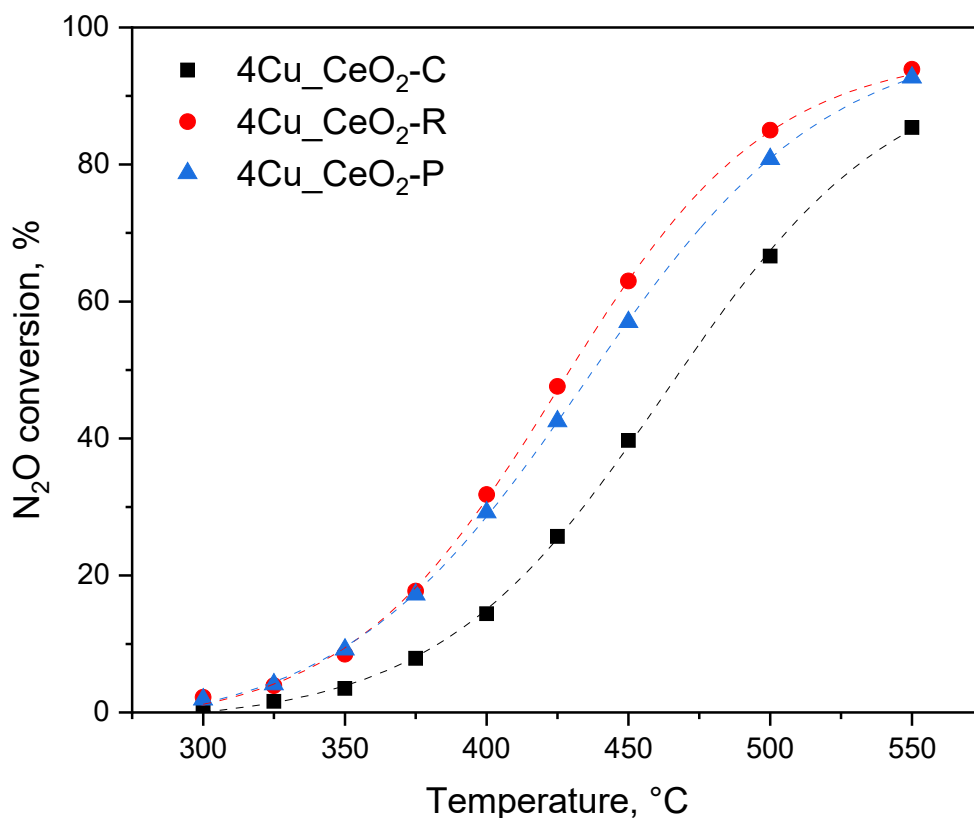


**Figure 2.** Results of catalytic N<sub>2</sub>O decomposition over 4Cu\_CeO<sub>2</sub>-C, 4Cu\_CeO<sub>2</sub>-R and 4Cu\_CeO<sub>2</sub>-P catalysts.

The observed difference in N<sub>2</sub>O decomposition TOF values over shaped ceria supports arises from higher oxygen mobility of CeO<sub>2</sub>-R and CeO<sub>2</sub>-C supports terminated with {100} and {110} high-energy surface planes, as was suggested in our previous study.<sup>[21]</sup>

### 3.2. Effect of copper content on N<sub>2</sub>O decomposition over Cu\_CeO<sub>2</sub>-R samples

As copper clusters supported on ceria nanorods possess the highest catalyst activity, we investigated the influence of different copper loadings (2-8 wt. % Cu) on catalytic activity and synergetic effect for this support (Figure 3).

With increasing copper loading, the formation of crystalline copper phase was observed only for the 8Cu\_CeO<sub>2</sub>-R sample (Figure S2). The results of dissociative N<sub>2</sub>O adsorption for this sample estimate the average copper particle size being 5.4 nm. At the same time, for materials

containing 2, 4 and 6 wt. % of Cu, copper phase is in highly dispersed state with the average size of clusters being equal to 1.8, 2.4 and 3.1 nm, respectively. Importantly, these samples containing up to 60 % of surface copper atoms (2Cu\_CeO<sub>2</sub>-R) allow to use the XAS method (which is a bulk analytical technique) to investigate catalytic processes taking place on the catalyst surface.

**Table 2.** Structural analysis and catalytic performance of Cu\_CeO<sub>2</sub>-R catalysts.

Sample	<sup>a</sup> d <sub>Cu</sub> , nm	<sup>b</sup> D <sub>Cu</sub> , %	<sup>c</sup> T <sub>50</sub> , °C	<sup>d</sup> Activity, mmol mol(Cu) <sup>-1</sup> min <sup>-1</sup>	<sup>e</sup> TOF, min <sup>-1</sup>
2-Cu_CeO <sub>2</sub> -R	1.8	60.2	490	32.4	0.054
4-Cu_CeO <sub>2</sub> -R	2.4	45.7	430	63.2	0.138
6-Cu_CeO <sub>2</sub> -R	3.1	35.0	420	48.8	0.139
8-Cu_CeO <sub>2</sub> -R	5.4	20.3	417	39.8	0.196

<sup>a</sup>Average particle size of copper and <sup>b</sup>dispersion of copper measured by means of dissociative N<sub>2</sub>O adsorption. <sup>c</sup>Temperature corresponding to 50 % of N<sub>2</sub>O conversion. <sup>d</sup>Activity obtained during catalytic N<sub>2</sub>O decomposition at 375 °C normalized per copper loading. <sup>e</sup>Turnover frequency was calculated by dividing moles of decomposed N<sub>2</sub>O at T=375 °C by moles of surface Cu atoms per unit time.

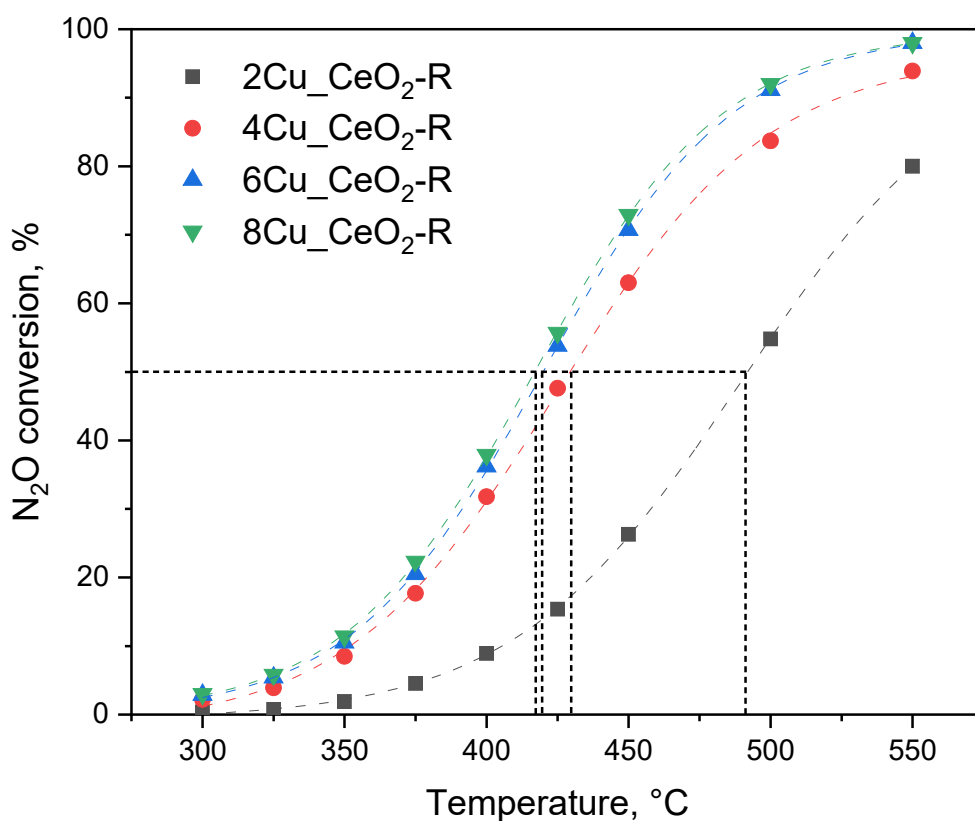


**Figure 3.** Results of catalytic N<sub>2</sub>O decomposition over catalysts containing 2-8 wt. % of copper on CeO<sub>2</sub>-R support.

The catalyst containing 2 wt. % of Cu despite high dispersion of copper shows significantly lower TOF values compared to other samples. The remaining three catalysts containing 4, 6 and 8 wt.% Cu, enabled higher and in the case of 6Cu-CeO<sub>2</sub>-R and 8Cu-CeO<sub>2</sub>-R samples, nearly identical N<sub>2</sub>O conversion. However, TOF values varied significantly (Table 2), revealing the 8Cu-CeO<sub>2</sub>-R sample containing intrinsically most active catalytic sites. This set of samples allows us to further investigate copper-ceria synergetic interaction and identify the main factor causing the unique properties of this highly investigated catalytic system. In order to investigate the origin of the so-called “synergetic effect” between copper and ceria phases, *in-situ* XAS analysis was applied.

### 3.3. *In-situ* Cu K-edge and Ce L<sub>3</sub>-edge XANES analysis

*In-situ* Cu K-edge and Ce L<sub>3</sub>-edge XANES analysis was used to reveal changes in valence of Cu and Ce species during CuO/CeO<sub>2</sub> catalyst activation in He flow (heating from room temperature to 400 °C) and during the N<sub>2</sub>O decomposition reaction (isothermal at 400 °C in 2500 ppm N<sub>2</sub>O/He flow).

Normalized Cu K-edge XANES spectra of the CuO/CeO<sub>2</sub> catalysts containing 2-8 wt. % of Cu deposited on CeO<sub>2</sub>-R and CeO<sub>2</sub>-C, measured *in-situ* during heating in He to 400 °C and during the catalytic reaction of N<sub>2</sub>O decomposition, are presented in the supplementary materials in Figures S3-S7, together with the spectra of corresponding Cu reference compounds.

The valence state of Cu cation can be determined from the energy position of the Cu K-edge. The changes in energy (about 4 eV) of the Cu K-edge is observed between Cu<sup>+</sup> and Cu<sup>2+</sup> cations, while a smaller edge shift of about 1 eV is exhibited between metallic Cu<sup>0</sup> and Cu<sup>+</sup> cation.<sup>[32–36]</sup> The energy position of Cu K-edge in all Cu modified CeO<sub>2</sub> catalysts with different CeO<sub>2</sub> morphologies and with different Cu loadings in the initial state at room temperature coincides with the energy position of Cu<sup>2+</sup> reference compounds (Figure S3), so we can conclude that Cu cations in the catalysts at room temperature are in divalent form.

The Cu K-edge XANES spectra measured *in-situ* during the catalyst activation in He atmosphere at 400 °C, clearly show the shift of the Cu K-edge to lower energies, indicating the reduction of Cu<sup>2+</sup> to Cu<sup>+</sup> and to metallic Cu<sup>0</sup> species. However, during the catalytic reaction of N<sub>2</sub>O decomposition at 400 °C a re-oxidation of copper species back to Cu<sup>2+</sup> oxidation state (Figures S3-S7) occurs. The PCA analysis of 26 XANES spectra measured during four *in-situ* N<sub>2</sub>O decomposition experiments over 8Cu\_CeO<sub>2</sub>-R, 4Cu\_CeO<sub>2</sub>-R, 2Cu\_CeO<sub>2</sub>-R, and 4Cu\_CeO<sub>2</sub>-C catalysts shows that a linear combination of up to four

different components is sufficient to completely describe each XANES spectrum in these series.

The relative amounts of  $\text{Cu}^{2+}$ ,  $\text{Cu}^{1+}$  and  $\text{Cu}^0$  species in the catalyst before and during the catalytic reaction at 400 °C were determined from the Cu K-edge XANES spectra, by the linear combination fit (LCF) analysis.<sup>[29]</sup> We attempted to identify the types of Cu bonding from the characteristic shape of the Cu K-edge profile. The best choices for the components with a physical meaning are XANES spectra measured on the reference Cu compounds, which are expected to be present in the samples. Four reference XANES profiles were identified that can reproduce all XANES spectra measured during *in-situ* experiment on different samples by a linear combination fit (LCF): the two spectra measured at RT on the initial state of the  $\text{CeO}_2$  nanorods with 8 wt.% and 2 wt.% Cu loading (samples 8Cu\_ $\text{CeO}_2$ -R and 2Cu\_ $\text{CeO}_2$ -R) as references for  $\text{Cu}^{2+}$ , and the spectrum of  $\text{Cu}_2\text{O}$  nanoparticles as reference for  $\text{Cu}^+$ , and Cu metal nanoparticles as reference for  $\text{Cu}^0$ . The spectra of  $\text{Cu}_2\text{O}$  and Cu metal nanoparticles were reconstructed directly from the set of *in-situ* spectra of the catalysts by Multivariate Curve Resolution analysis.<sup>[29,37]</sup> Examples of LCF analysis are presented in the supplementary materials (Figures S8-S9). The relative amount of each reference spectrum obtained in LCF corresponds to a relative amount of each  $\text{Cu}^0$ ,  $\text{Cu}^+$  and  $\text{Cu}^{2+}$  species in the sample. The results are shown in Figure 4.

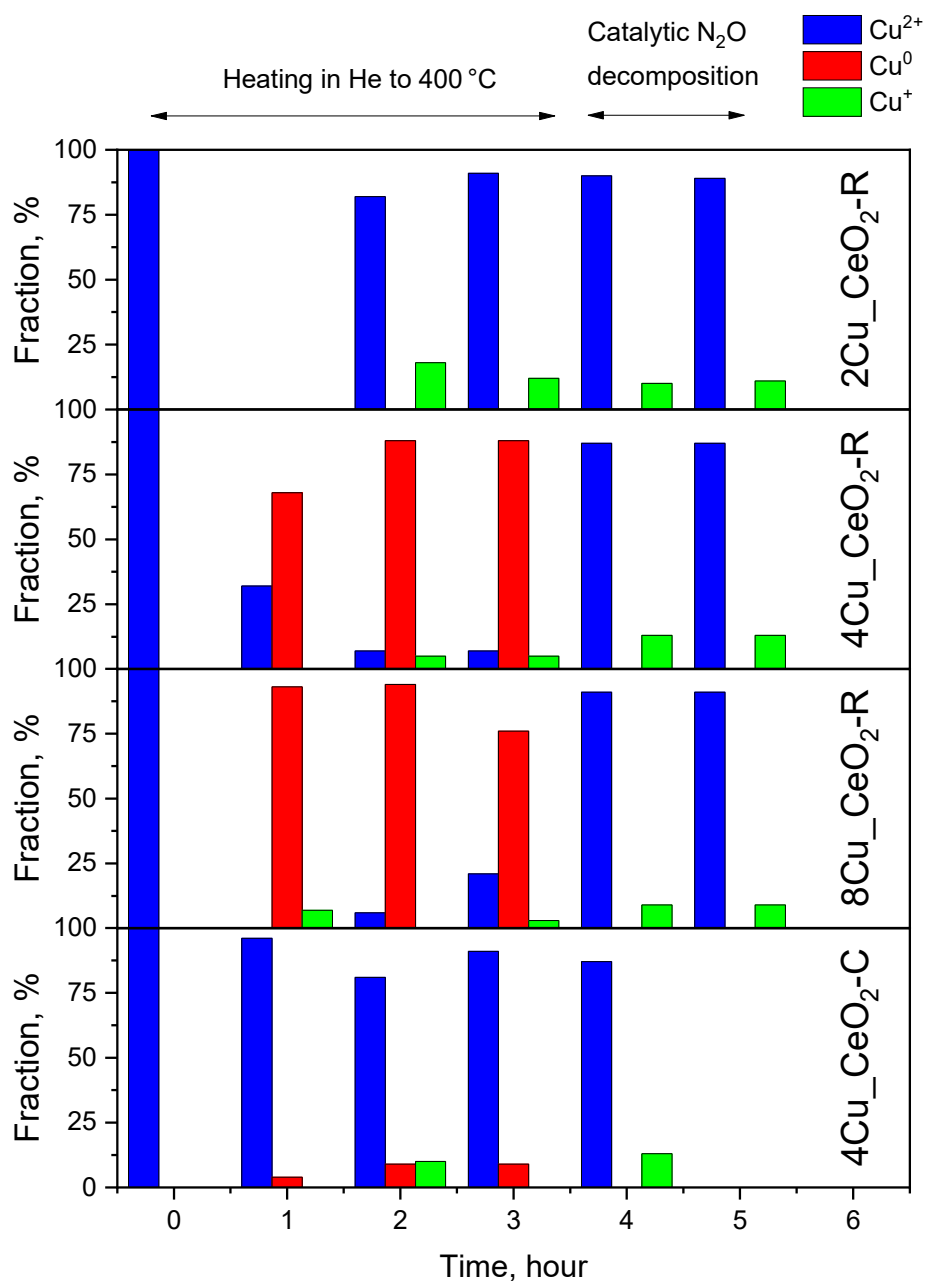


**Figure 4.** Relative amounts of Cu<sup>2+</sup>, Cu<sup>+</sup> and Cu<sup>0</sup> oxidation states in different Cu/CeO<sub>2</sub> samples at 25 °C, during heating in He to 400 °C, and during catalytic N<sub>2</sub>O decomposition at 400 °C, determined by LCF analysis of *in-situ* Cu K-edge XANES spectra.

Before the catalytic reaction at room temperature, all copper is present as Cu<sup>2+</sup> in all samples. During the activation in He as well as during catalytic N<sub>2</sub>O decomposition Cu valence state

changes significantly. The temporal evolution of the  $\text{Cu}^0$ ,  $\text{Cu}^+$  and  $\text{Cu}^{2+}$  fractions strongly depend on  $\text{CeO}_2$  morphology and on Cu size.

In the case of  $\text{CeO}_2$  nanorods with high Cu loading (8Cu\_ $\text{CeO}_2$ -R and 4Cu\_ $\text{CeO}_2$ -R,) we observe that during heating in He at 400 °C, a significant part of  $\text{Cu}^{2+}$  ( $\approx 70$ –80 %) is reduced to metallic copper (Figure 4). This is in good agreement with previously reported data, where CuO reduction to  $\text{Cu}^+$  and  $\text{Cu}^0$  state was observed by CO-DRIFTS after CuO/ $\text{CeO}_2$  catalyst pre-treatment in  $\text{N}_2$  at 300 °C.<sup>[21]</sup> During the catalytic  $\text{N}_2\text{O}$  decomposition at 400 °C, almost all Cu is oxidized back to  $\text{Cu}^{2+}$ , and only a small fraction (about 9-13 %) of  $\text{Cu}^+$  is formed. In contrast, activation of another two samples (i.e. 4Cu\_ $\text{CeO}_2$ -C and 2Cu\_ $\text{CeO}_2$ -R) in helium at 400 °C, did not result in formation of metallic copper species. Furthermore, we have observed partial re-oxidation of copper for the 2Cu\_ $\text{CeO}_2$ -R sample. We attribute this behavior to the accompanying process of ceria reduction in the same temperature range (Figure 5) due to EMSI between copper and ceria support. Namely, for the 2Cu\_ $\text{CeO}_2$ -R sample, the fraction of reduced copper species reaches 10 % in equilibrium state in He at 400 °C, and this value remains constant also during the catalytic  $\text{N}_2\text{O}$  decomposition. In case of 4Cu\_ $\text{CeO}_2$ -C catalyst, insignificant reduction of CuO to metallic copper (less than 20 % of CuO was reduced) is observed during heating in He to 400 °C. Also, there are no significant changes in the Cu valence state during the catalytic reaction. Cu remains in the divalent form, co-existing with about 13 % of  $\text{Cu}^+$ .

Normalized Ce L<sub>3</sub>-edge XANES spectra of the 4Cu\_ $\text{CeO}_2$ -R catalyst, measured *in-situ* during heating in He to 400 °C, and during the catalytic reaction of  $\text{N}_2\text{O}$  decomposition, are shown in Figure S10, together with the spectra of corresponding Ce reference compounds.

The energy position of Ce L<sub>3</sub>-edge and the edge profile in the 4Cu- $\text{CeO}_2$ -R catalyst in initial state at room temperature coincides with the energy position and edge profile of crystalline  $\text{CeO}_2$ , indicating that Ce cations in the catalyst are in  $\text{Ce}^{4+}$  valence state. The Ce L<sub>3</sub>-edge in

XANES spectra measured *in-situ* during catalyst activation in He atmosphere at 400 °C are slightly shifted to lower energies, indicating the partial reduction of  $\text{Ce}^{4+}$  to  $\text{Ce}^{3+}$ . During the catalytic reaction of  $\text{N}_2\text{O}$  decomposition at 400 °C a re-oxidation of Ce species back to  $\text{Ce}^{4+}$  oxidation state is observed (Figure S10).

The relative amounts of  $\text{Ce}^{4+}$  and  $\text{Ce}^{3+}$  species in the catalyst before and during the catalytic reaction at 400 °C (Figure 5) were determined from the Ce  $\text{L}_3$ -edge XANES spectra by the linear combination fit (LCF) analysis.<sup>[29,38]</sup> The spectra can be completely described by a linear combination of up to two components: Ce  $\text{L}_3$ -edge XANES profile of the sample 4Cu\_CeO<sub>2</sub>-R catalyst in initial state at RT as reference for  $\text{Ce}^{4+}$ , and XANES of crystalline  $\text{CeVO}_4$  as reference for  $\text{Ce}^{3+}$ . The results of LCF are given in Figure 5. An example of LCF analysis is illustrated in Figure S11.

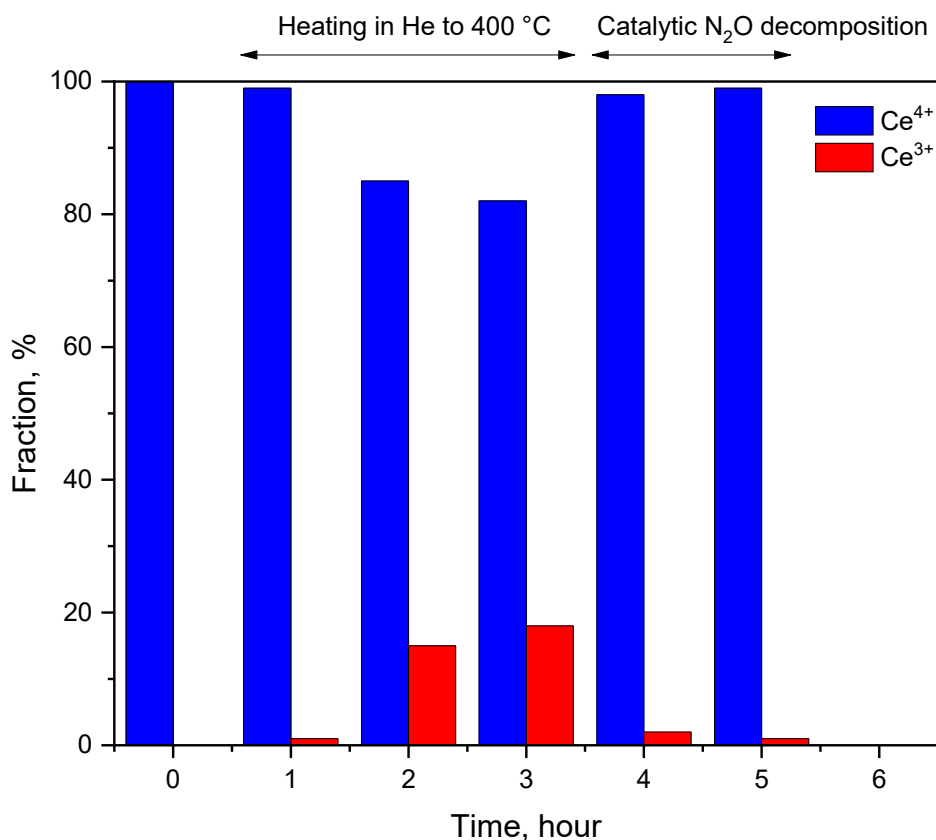


**Figure 5.** Relative amounts of Ce<sup>4+</sup> and Ce<sup>3+</sup> oxidation states in 4Cu\_CeO<sub>2</sub>-R sample at 25 °C, during heating in He to 400 °C, and during catalytic N<sub>2</sub>O decomposition at 400 °C, determined by LCF analysis of *in-situ* Ce L<sub>3</sub>-edge XANES spectra.

In the initial state at room temperature (25 °C), cerium is present exclusively as Ce<sup>4+</sup>. During heating in He to 400 °C, about 15 % of Ce<sup>4+</sup> is reduced to Ce<sup>3+</sup> (Figure 5). After switching from He to 2500 ppm N<sub>2</sub>O in He at 400 °C, only about 1 % of cerium is retained in the reduced Ce<sup>3+</sup> form accordingly to LCF analysis. Taking into account the dimensions of CeO<sub>2</sub> nanorods (average diameter of 8 nm and length between 80 and 140 nm), we can estimate that the reduction of ceria during heating to 400 °C is limited to about two unit cells of CeO<sub>2</sub> nanoparticles.

### 3.3. *In-situ* Cu K-edge EXAFS analysis

*In-situ* Cu K-edge EXAFS analysis was used to determine average local structure around copper cations in the Cu modified ceria nanocubes and nanorods and different Cu loadings in the range from 2 to 8 wt. %. We investigated the changes in local structure during heating to 400 °C in He atmosphere, as well as during N<sub>2</sub>O decomposition reaction at 400 °C. In Fourier transform magnitude of the EXAFS spectra (Figures S12-S16) the contributions of photoelectron scattering on the nearest shells of neighbors around the Cu atoms are observed in the R range up to about 4 Å. In all cases, a strong peak in the R range between 1 Å and 2.2 Å can be attributed to photoelectron backscattering on the nearest oxygen neighbors around Cu. Weaker peaks in the R range between 2.3 Å and 3.6 Å represent the contributions from more distant Cu coordination shells. Qualitative comparisons of the FT spectra show the difference in average Cu neighborhoods between the catalyst with different Cu loadings and different CeO<sub>2</sub> morphologies already in the initial state (Figure S12). The series of *in-situ* EXAFS spectra for each catalyst sample reveal structural changes that appear after heating of the samples at 400 °C in He atmosphere, and then during the catalytic reaction of N<sub>2</sub>O decomposition (Figures S13-S16).

As indicated by Cu K-edge XANES results, we can expect mixtures of different Cu species in the catalysts. In the initial state at RT all copper cations are expected to be in a divalent state bound in CuO nanoclusters or amorphous CuO oxides attached to the surface of CeO<sub>2</sub> nanoparticles. During catalyst activation in He atmosphere at 400 °C, where the reduction of Cu<sup>2+</sup> is observed mainly to metallic Cu<sup>0</sup> species, and in some cases partially to Cu<sup>+</sup> species, we can expect a mixture of divalent and monovalent copper oxide nanoparticles and metallic copper nanoparticles on the surface of ceria support. During the catalytic reaction of N<sub>2</sub>O decomposition at 400 °C, where a re-oxidation of almost all Cu species back to Cu<sup>2+</sup> is found,

we can expect again a mixture of divalent copper oxide species on the surface of ceria support.

Structural parameters of the average local Cu neighborhood (type and average number of neighbors, the radii and Debye-Waller factor of neighbor shells) are quantitatively resolved from the EXAFS spectra by comparing the measured EXAFS signal with the model signal, constructed *ab initio* with the FEFF6 program code.<sup>[30]</sup> A combined FEFF model is used, composed of neighbor atoms at distances characteristic for the expected Cu oxide and Cu metal species that may be present in the samples. The atomic species of neighbors are identified in the fit by their specific scattering factor and phase shift. Details of the quantitative EXAFS analysis are presented in the supporting materials.

With EXAFS analysis it is not possible to unambiguously identify all Cu species in the mixture and determine their structures. The proposed FEFF model aims to describe the average Cu local neighborhood in the initial state and identify the main structural changes before and during the catalytic reaction at 400 °C. The nearest coordination shell comprised of oxygen atoms. Cu, Ce and oxygen neighbors are included in more distant coordination shells at distances characteristic for the expected Cu oxide and Cu metal species attached to the CeO<sub>2</sub> surface.

A good agreement between the model and the experimental spectra is found using the k range of 3 Å<sup>-1</sup> to 12 Å<sup>-1</sup> and the R range of 1.0 Å to 4.0 Å. Representative in situ FT EXAFS spectra of the 8Cu\_CeO<sub>2</sub>-R catalyst with best fit EXAFS models are shown in Figure 6. Best fit results for all in-situ EXAFS spectra of all samples are presented in the supporting materials (Figures S13-S16). The list of best fit parameters is given in the Tables S4-S15. The uncertainties of the best fit parameters N and  $\sigma^2$  of more distant coordination shells are relatively large due to correlations between these parameters. Structural parameters of three

reference crystalline Cu compounds (CuO, Cu<sub>2</sub>O and metallic Cu) obtained by EXAFS analysis are presented in Table S1-S3 for comparison.

Results of EXAFS analysis (Tables S1-S15) show that in all studied catalysts at RT copper cations are coordinated to oxygen atoms in the first coordination shell and Cu neighbors in more distant coordination shells, at distances characteristic for copper oxide tenorite phase (Figure 6). The coordination numbers are significantly lower than in the bulk CuO (Table S1), indicating that CuO is in the form of small nanoparticles. This is in good agreement with the results of dissociative N<sub>2</sub>O chemisorption, where the size of copper clusters varied in the range from 2.1 to 5.1 nm (Table 1). In addition, we observe the presence of Cu-Ce photoelectron scattering at  $\approx 3.16$  Å, indicating that part of Cu cations is in the immediate vicinity of ceria surface forming Cu-O-Ce bridges. Furthermore, the average number of Ce neighbors determined at RT decreased from 1.2 to 0.2 with increasing copper content in the samples from 2 to 8 wt. % (Tables S4, S7 and S10). Thus, we can clearly conclude that increasing of copper loading influences not only copper nanoparticle size, but also the length of the interface between copper and ceria phases, which according to previous studies might play a critical role in N<sub>2</sub>O decomposition <sup>[39]</sup>. Overall, the results of EXAFS analysis at RT strongly support the XANES findings: Cu cations in all catalyst samples are in the form of divalent CuO nanoparticles and/or amorphous oxide species and attached to the surface of CeO<sub>2</sub> nanoparticles.

During heating of the catalyst samples to 400 °C in He atmosphere and during catalytic N<sub>2</sub>O decomposition at 400 °C, significantly different behavior is observed for CeO<sub>2</sub>-R based catalysts with higher Cu loadings (8 and 4 wt. %) compared to those with lower (2 wt.%) Cu loading (2Cu\_CeO<sub>2</sub>-R) and CeO<sub>2</sub>-C based catalyst containing 4 wt.% Cu (4Cu\_CeO<sub>2</sub>-C).

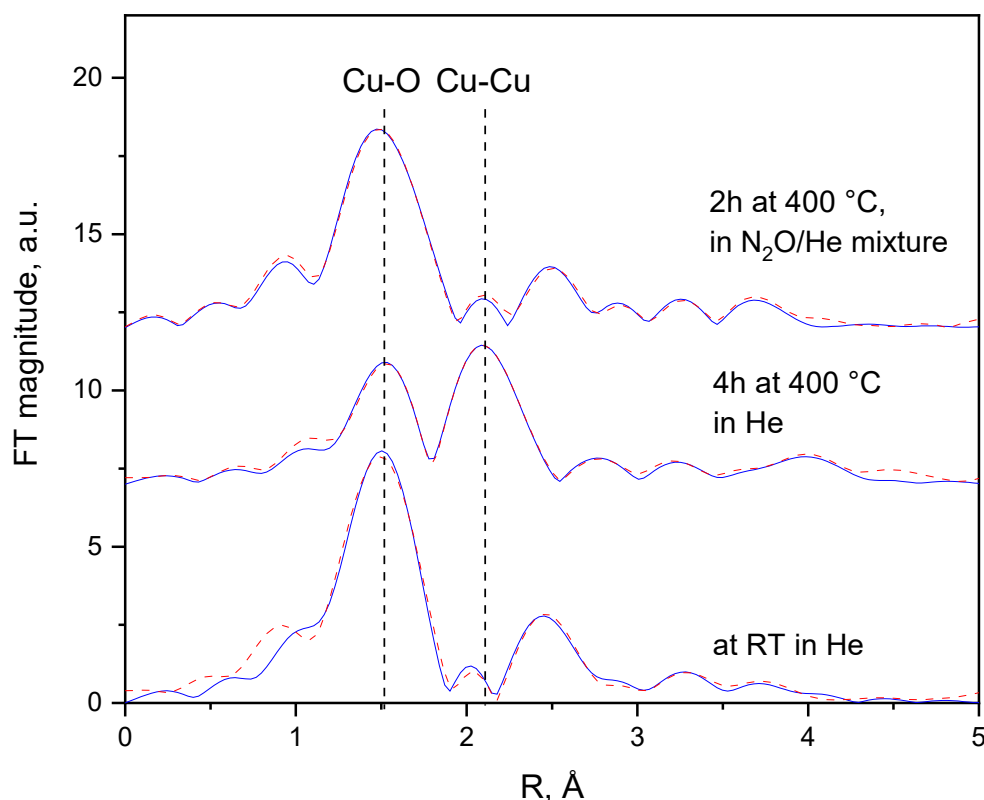


**Figure 6.** Representative Fourier transform magnitude of  $k^3$ -weighted Cu EXAFS spectra of the 8Cu\_CeO<sub>2</sub>-R catalyst at room temperature as well as measured *in-situ* during heating in He at 400 °C, and during catalytic N<sub>2</sub>O decomposition at 400 °C, calculated in the  $k$  range of 3–12 Å<sup>-1</sup> and  $R$  range of 1 to 3.5 Å. Experiment – (solid line); model -- (dashed line). Spectra are shifted vertically for clarity. The positions of nearest oxygen and nearest copper neighbour peaks are indicated by vertical dashed lines.

In the 8Cu\_CeO<sub>2</sub>-R and 4Cu\_CeO<sub>2</sub>-R catalysts, CuO is transformed to small metallic Cu nanoparticles during heating to 400 °C in He atmosphere. The Cu-Cu interatomic distances revealed during EXAFS fitting are characteristic for Cu metal with the fcc crystal structure (Figure 6); however, the coordination numbers are significantly lower than in the bulk metallic Cu pointing out the formation of metallic copper nanoparticles containing a large fraction of coordinatively unsaturated surface atoms (Tables S5 and S8). The abovementioned

results are in good agreement with the results of XANES analysis (Figure 4), which showed that during heating in He to 400 °C, a significant part (80-90 %) of  $\text{Cu}^{2+}$  is reduced to metallic  $\text{Cu}^0$  nanoparticles.

In contrast to the previous two samples, EXAFS analysis of the  $2\text{Cu\_CeO}_2\text{-R}$  and  $4\text{Cu\_CeO}_2\text{-C}$  shows that during heating in He at 400 °C Cu cations predominantly remain in the form of different CuO nanoparticles and/or amorphous oxide species attached to the surface of  $\text{CeO}_2$  nanoparticles. This indicates that when heated in He, small CuO clusters having a higher fraction of Cu-O-Ce bonds are actually more difficult to reduce compared to larger CuO crystallites. This is in contrast to often-reported information in the literature, where  $\text{H}_2$ -TPR profiles are interpreted (without actual analysis of copper or cerium oxidation states) in a sense that the low-temperature peak belongs to the reduction of small CuO clusters, whereas high-temperature reduction peak is assigned to larger CuO crystals.<sup>[40]</sup> Also, the shape of  $\text{CeO}_2$  and possibly the terminating facets appear to govern or initiate the reduction of CuO phase. On  $4\text{Cu\_CeO}_2\text{-C}$  and  $8\text{-Cu-CeO}_2\text{-R}$  catalysts which contain CuO particles of very similar average size (5.1 and 5.4 nm, respectively), CuO remains oxidized on  $\text{CeO}_2\text{-C}$ , whereas is reduced extensively on  $\text{CeO}_2\text{-R}$ . During catalytic  $\text{N}_2\text{O}$  decomposition at 400 °C, the average local structure around Cu cations for all investigated samples indicates that majority of Cu cations are re-oxidized to different CuO nanoparticles and/or amorphous oxide species attached to  $\text{CeO}_2$  support. This is in line with the results of XANES analysis (Figure 4).

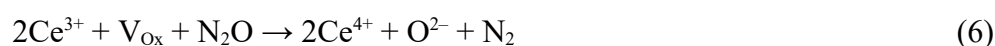
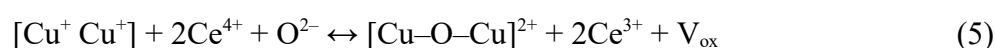
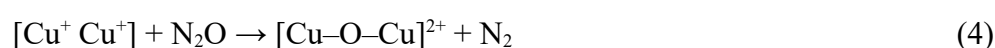
During catalyst activation in He and catalytic  $\text{N}_2\text{O}$  decomposition (both at 400 °C) we further observed significant changes in Cu-Ce coordination numbers (Tables S4-S15). It was found that heating in He leads to a decrease of Ce neighbor atoms indicating shrinkage of the ceria-copper interface. However, (in oxidative atmosphere) during  $\text{N}_2\text{O}$  decomposition, we observed that coordination number for Cu-Ce photoelectron scattering not only restores its initial values (RT in He flow), but also for some catalyst exceeds it more than 3 times, which

indicates a drastic increase of copper-ceria interface.

### 3.4. Discussion

*In-situ* XAS data collected during catalyst activation in helium and during catalytic N<sub>2</sub>O decomposition at 400 °C highlight the crucial role of both ceria support and copper in the catalytic cycle of N<sub>2</sub>O decomposition. In our previous work,<sup>[25]</sup> we identified the presence of reduced Ce<sup>3+</sup> species and bent mono(oxo) dicopper sites under reaction conditions. Furthermore, we propose that mono(oxo) dicopper species undergo reduction during the catalytic cycle and form reduced Cu<sup>+</sup> species, which are the active sites and can activate the N<sub>2</sub>O molecule. However, due to limitations of UV-Vis DR and FTIR spectroscopies, we were not able to detect these reduced copper species and therefore, the species participating in N<sub>2</sub>O degradation were not precisely established. By applying XAS spectroscopy, which is an appropriate technique to determine oxidation state and local geometry of investigated atoms, we finally observed reduced Cu<sup>+</sup> species under reaction conditions and obtained solid evidence of involvement of Cu<sup>2+</sup>/Cu<sup>+</sup> pair in the catalytic cycle. Taking into account the results of *in-situ* XAS experiment and actual copper loading in these samples, we have calculated the amount of reduced Cu<sup>+</sup> species presented in Cu-CeO<sub>2</sub>-R catalysts during catalytic N<sub>2</sub>O decomposition. Figure S17 shows a good correlation between the activity of these catalysts at 400 °C and determined Cu<sup>+</sup> content in these samples. These data unambiguously confirm previous findings, where the involvement of Cu<sup>2+</sup>/Cu<sup>+</sup> redox pair was suggested.<sup>[25]</sup>

Previously proposed redox mechanism of N<sub>2</sub>O decomposition (Equations 3-6) predicted oxygen evolution from bent mono(oxo) dicopper sites and Cu<sup>+</sup> sites formation (Equation 3), as a key step in the reaction mechanism. During *in-situ* XAS study, we have simulated experimental conditions where such reactions should take place. We found that catalyst heating in inert gas atmosphere (Figure 4) shifts the reaction equilibrium between different copper oxidation states to reduced copper species (Cu<sup>+</sup> and Cu<sup>0</sup>). We observed that the investigated materials undergo reduction during catalyst pretreatment and a significant part of copper before the introduction of N<sub>2</sub>O is in reduced state for most active 4Cu\_CeO<sub>2</sub>-R and 8Cu\_CeO<sub>2</sub>-R samples. This fact is in good agreement with our previous work,<sup>[25]</sup> where we have suggested that oxygen evolution and formation of reduced copper species is a rate-limiting step in this catalytic cycle and as such ability of the catalyst to form reduced copper species is crucial during catalytic cycle of N<sub>2</sub>O degradation. Here, we found that the 4Cu\_CeO<sub>2</sub>-R sample easily evolves oxygen and thus re-generates sites for N<sub>2</sub>O activation and decomposition, and consequently possesses high N<sub>2</sub>O decomposition rate.



As soon as N<sub>2</sub>O was introduced into the feed gas, we have immediately observed oxidation of both copper and ceria (Equations 4 and 6), correspondingly. Only a small fraction of copper remains in the Cu<sup>+1</sup> oxidation state under steady-state conditions for all the samples. At the relatively low reaction temperature (400 °C), the overall kinetics of N<sub>2</sub>O decomposition is limited by oxygen desorption step and therefore both cerium support and copper are mostly

oxidized. At the same time, the presence of both  $\text{Cu}^+$  and  $\text{Ce}^{3+}$  reduced species even in relatively small fractions, confirms the participation of both  $\text{Cu}^+/\text{Cu}^{2+}$  and  $\text{Ce}^{3+}/\text{Ce}^{4+}$  in the catalytic cycle as was suggested before. Our work further confirms the importance of electronic metal support interactions (EMSI) as it was found to take place in this system.<sup>[26,41–44]</sup> The perturbations in the electronic properties of Cu and Ce *via* bonding interaction between copper nanoparticles and ceria support directly affect the reducibility of both of these phases.<sup>[42]</sup> As such, the improved reducibility and oxygen mobility result in outstanding catalytic performance of Cu/CeO<sub>2</sub> system in the catalytic N<sub>2</sub>O decomposition reaction.<sup>[43]</sup> Finally, by using *in-situ* EXAFS analysis we have shown that the investigated copper-ceria materials represent a dynamic system under N<sub>2</sub>O decomposition conditions. The increased interface between copper and ceria phases under catalytic N<sub>2</sub>O decomposition reaction conditions results in the ability of CuO-CeO<sub>2</sub> catalyst to decompose N<sub>2</sub>O already at moderate temperatures.

#### 4. Conclusions

With *in-situ* XAS analysis of nanoshaped CuO/CeO<sub>2</sub> catalysts during N<sub>2</sub>O decomposition, we identified structural characteristics and changes of Cu and Ce species during catalytic reaction. The Cu K-edge and Ce L<sub>3</sub>-edge XANES and EXAFS analyses revealed changes in valence and local structure of Cu and Ce species in the CuO/CeO<sub>2</sub> catalysts. In the initial state at RT, the  $\text{Cu}^{2+}$  cations are in the form of CuO nanoparticles attached to the CeO<sub>2</sub> surface. After heating at 400 °C in He, partial (~15 %) reduction of  $\text{Ce}^{4+}$  is detected, and a significant part of  $\text{Cu}^{2+}$  is reduced to  $\text{Cu}^+$  and  $\text{Cu}^0$ . During the catalytic reaction of N<sub>2</sub>O decomposition, a major part of  $\text{Ce}^{3+}$  is oxidized back to  $\text{Ce}^{4+}$ , and a significant part of Cu species is oxidized back to  $\text{Cu}^{2+}$ , with about 10 % of  $\text{Cu}^+$  remaining in reduced state under steady-state

conditions. Observed structural and valence changes confirm the participation of both  $\text{Cu}^+/\text{Cu}^{2+}$  and  $\text{Ce}^{3+}/\text{Ce}^{4+}$  ionic pairs in the catalytic cycle of  $\text{N}_2\text{O}$  decomposition. Furthermore, *in-situ* EXAFS analysis revealed highly dynamic changes in copper-ceria interface: Under oxidizing reaction conditions, the catalyst undergoes re-shaping in order to increase the copper-ceria interface.

**Acknowledgements** - The authors gratefully acknowledge the financial support of the Slovenian Research Agency through Research programs P1-0112, P2-0150 and P2-0393, and by the project CALIPSOplus under the Grant Agreement 730872 from the EU Framework Programme for Research and Innovation HORIZON 2020. We acknowledge access to the SR facilities of ELETTRA (beamline XAFS, pr. 20165258) and PETRAIII (beamline P65, pr. I-20160044 EC and I-20180898 EC) at DESY, a member of the Helmholtz Association (HGF). We would like to thank Edmund Welter of PETRA III and Giuliana Aquilanti of ELETTRA for expert advice on beamline operation and for assistance during the experiment.

## References

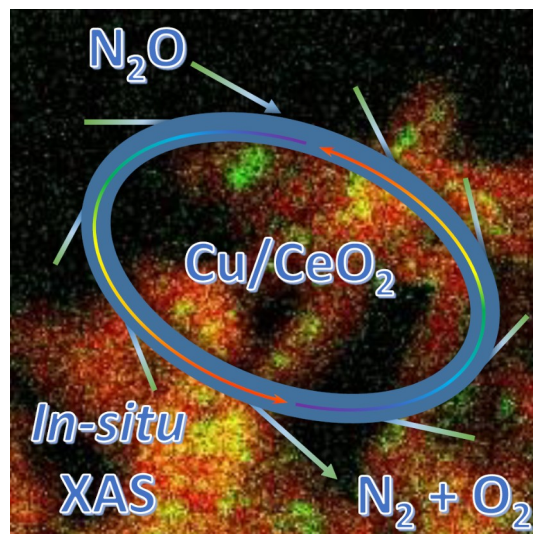
- [1] L. Xue, C. Zhang, H. He, Y. Teraoka, *Catal. Today* **2007**, 126, 449–455.
- [2] D. J. Wuebbles, *Science (80-. )*. **2009**, 326, 56–57.
- [3] E. A. Davidson, D. Kanter, *Environ. Res. Lett.* **2014**, 9, 105012.
- [4] R. Amrousse, A. Tsutsumi, A. Bachar, *Catal. Sci. Technol.* **2013**, 3, 576–579.
- [5] M. Hussain, D. Fino, N. Russo, *Chem. Eng. J.* **2014**, 238, 198–205.
- [6] M. Piumetti, M. Hussain, D. Fino, N. Russo, *Appl. Catal. B Environ.* **2015**, 165, 158–168.
- [7] E. M. Jabłońska, L. Buselli, E. M. Nocuń, R. Palkovits, *ChemCatChem* **2018**, 10, 296–

- [8] H. Zhu, Y. Li, X. Zheng, *Appl. Catal. A Gen.* **2019**, 571, 89–95.
- [9] Z. Liu, C. He, B. Chen, H. Liu, *Catal. Today* **2017**, 297, 78–83.
- [10] M. Lykaki, E. Papista, S. A. C. Carabineiro, P. B. Tavares, M. Konsolakis, *Catal. Sci. Technol.* **2018**, 8, 2312–2322.
- [11] M. Jabłońska, M. A. Arán, A. M. Beale, K. Góra-Marek, G. Delahay, C. Petitto, K. Pacultová, R. Palkovits, *RSC Adv.* **2019**, 9, 3979–3986.
- [12] S. Gudyka, G. Grzybek, J. Gryboś, P. Indyka, B. Leszczyński, A. Kotarba, Z. Sojka, *Appl. Catal. B Environ.* **2017**, 201, 339–347.
- [13] J. Bin Lim, S. H. Cha, S. B. Hong, *Appl. Catal. B Environ.* **2019**, 243, 750–759.
- [14] D. Pietrogiacomì, M. C. Campa, L. R. Carbone, M. Occhiuzzi, *Appl. Catal. B Environ.* **2019**, 240, 19–29.
- [15] P. Stelmachowski, G. Maniak, J. Kaczmarczyk, F. Zasada, W. Piskorz, A. Kotarba, Z. Sojka, *Appl. Catal. B Environ.* **2014**, 146, 105–111.
- [16] G. Grzybek, P. Stelmachowski, S. Gudyka, J. Duch, K. Ćmil, A. Kotarba, Z. Sojka, *Appl. Catal. B Environ.* **2015**, 168–169, 509–514.
- [17] F. Zasada, W. Piskorz, J. Janas, J. Gryboś, P. Indyka, Z. Sojka, *ACS Catal.* **2015**, 6879–6892.
- [18] Y. Wu, C. Cordier, E. Berrier, N. Nuns, C. Dujardin, P. Granger, *Appl. Catal. B Environ.* **2013**, 140–141, 151–163.
- [19] D. V. Ivanov, L. G. Pinaeva, L. A. Isupova, E. M. Sadovskaya, I. P. Prosvirin, E. Y. Gerasimov, I. S. Yakovleva, *Appl. Catal. A Gen.* **2013**, 457, 42–51.
- [20] M. Zabilskiy, B. Erjavec, P. Djinić, A. Pintar, *Chem. Eng. J.* **2014**, 254, 153–162.
- [21] M. Zabilskiy, P. Djinić, E. Tchernychova, O. P. Tkachenko, L. M. Kustov, A. Pintar, *ACS Catal.* **2015**, 5, 5357–5365.

- [22] M. Zabilskiy, P. Djinović, B. Erjavec, G. Dražić, A. Pintar, *Appl. Catal. B Environ.* **2015**, *163*, 113–122.
- [23] A. Adamski, W. Zajac, F. Zasada, Z. Sojka, *Catal. Today* **2012**, *191*, 129–133.
- [24] M. I. Konsolakis, S. A. C. Carabineiro, E. Papista, G. E. Marnellos, P. B. Tavares, J. Agostinho Moreira, Y. Romaguera-Barcelay, J. L. Figueiredo, *Catal. Sci. Technol.* **2015**, 3714–3727.
- [25] M. Zabilskiy, P. Djinović, E. Tchernychova, A. Pintar, *Appl. Catal. B Environ.* **2016**, *197*, 146–158.
- [26] M. Lykaki, E. Pachatouridou, S. A. C. Carabineiro, E. Iliopoulou, C. Andriopoulou, N. Kallithrakas-Kontos, S. Boghosian, M. Konsolakis, *Appl. Catal. B Environ.* **2018**, *230*, 18–28.
- [27] X. Shen, L. J. Garces, Y. Ding, K. Laubernds, R. P. Zerger, M. Aindow, E. J. Neth, S. L. Suib, *Appl. Catal. A Gen.* **2008**, *335*, 187–195.
- [28] A. Dandekar, M. A. Vannice, *J. Catal.* **1998**, *178*, 621–639.
- [29] B. Ravel, M. Newville, IUCr, *J. Synchrotron Radiat.* **2005**, *12*, 537–541.
- [30] J. J. Rehr, R. C. Albers, S. I. Zabinsky, *Phys. Rev. Lett.* **1992**, *69*, 3397–3400.
- [31] M. Nolan, S. C. Parker, G. W. Watson, *Surf. Sci.* **2005**, *595*, 223–232.
- [32] J. Teržan, P. Djinović, J. Zavašnik, I. Arčon, G. Žerjav, M. Spreitzer, A. Pintar, *Appl. Catal. B Environ.* **2018**, *237*, 214–227.
- [33] A. Manceau, A. Matynia, *Geochim. Cosmochim. Acta* **2010**, *74*, 2556–2580.
- [34] W. W. Wang, W. Z. Yu, P. P. Du, H. Xu, Z. Jin, R. Si, C. Ma, S. Shi, C. J. Jia, C. H. Yan, *ACS Catal.* **2017**, *7*, 1313–1329.
- [35] E. M. C. Alayon, M. Nachtegaal, A. Bodi, M. Ranocchiari, J. A. Van Bokhoven, *Phys. Chem. Chem. Phys.* **2015**, *17*, 7681–7693.
- [36] T. Čižmar, U. Lavrenčič Štangar, M. Fanetti, I. Arčon, *ChemCatChem* **2018**, *10*, 2982–

2993.

- [37] A. Scafuri, R. Berthelot, K. Pirnat, A. Vizintin, J. Bitenc, G. Aquilanti, D. Foix, R. Dedryvère, I. Arčon, R. Dominko, et al., *Chem. Mater.* **2020**, 32, 8266–8275.
- [38] T. Thajudheen, A. G. Dixon, S. Gardonio, I. Arčon, M. Valant, *J. Phys. Chem. C* **2020**, 124, 19929–19936.
- [39] P. Alvarez, G. Aguila, S. Guerrero, P. Araya, *J. Chil. Chem. Soc.* **2018**, 63, 4102–4108.
- [40] M. F. Luo, Y. J. Zhong, X. X. Yuan, X. M. Zheng, *Appl. Catal. A Gen.* **1997**, 162, 121–131.
- [41] C. T. Campbell, *Nat. Chem.* **2012**, 4, 597–598.
- [42] M. Konsolakis, *Appl. Catal. B Environ.* **2016**, 198, 49–66.
- [43] M. I. Konsolakis, *ACS Catal.* **2015**, 5, 6397–6421.
- [44] M. Konsolakis, M. Lykaki, *Catalysts* **2020**, 10, 160.



*In-situ* XAS study of  $\text{N}_2\text{O}$  decomposition over  $\text{CuO/CeO}_2$  catalysts revealed the crucial role of copper-ceria interface and participating of  $\text{Cu}^{2+}/\text{Cu}^+$  and  $\text{Ce}^{4+}/\text{Ce}^{3+}$  ionic pairs in the catalytic cycle.